Accepted Manuscript

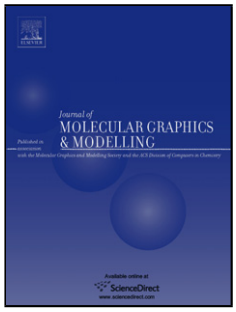

Title: The Unbinding Studies of Vascular Endothelial Growth Factor Receptors-2 Protein Tyrosine Kinase Type II Inhibitors

Author: Cong-min Kang Dong-qing Liu Xin-ying Wang Ri-lei Yu Ying-tao Lv

PII: S1093-3263(15)00077-7
DOI: http://dx.doi.org/doi:10.1016/j.jmgm.2015.04.011
Reference: JMG 6539

To appear in: *Journal of Molecular Graphics and Modelling*

Received date: 26-3-2015
Revised date: 17-4-2015
Accepted date: 20-4-2015

Please cite this article as: <doi>http://dx.doi.org/10.1016/j.jmgm.2015.04.011</doi>

This is a PDF file of an unedited manuscript that has been accepted for publication. As a service to our customers we are providing this early version of the manuscript. The manuscript will undergo copyediting, typesetting, and review of the resulting proof before it is published in its final form. Please note that during the production process errors may be discovered which could affect the content, and all legal disclaimers that apply to the journal pertain.

Graphical Abstract (for review)

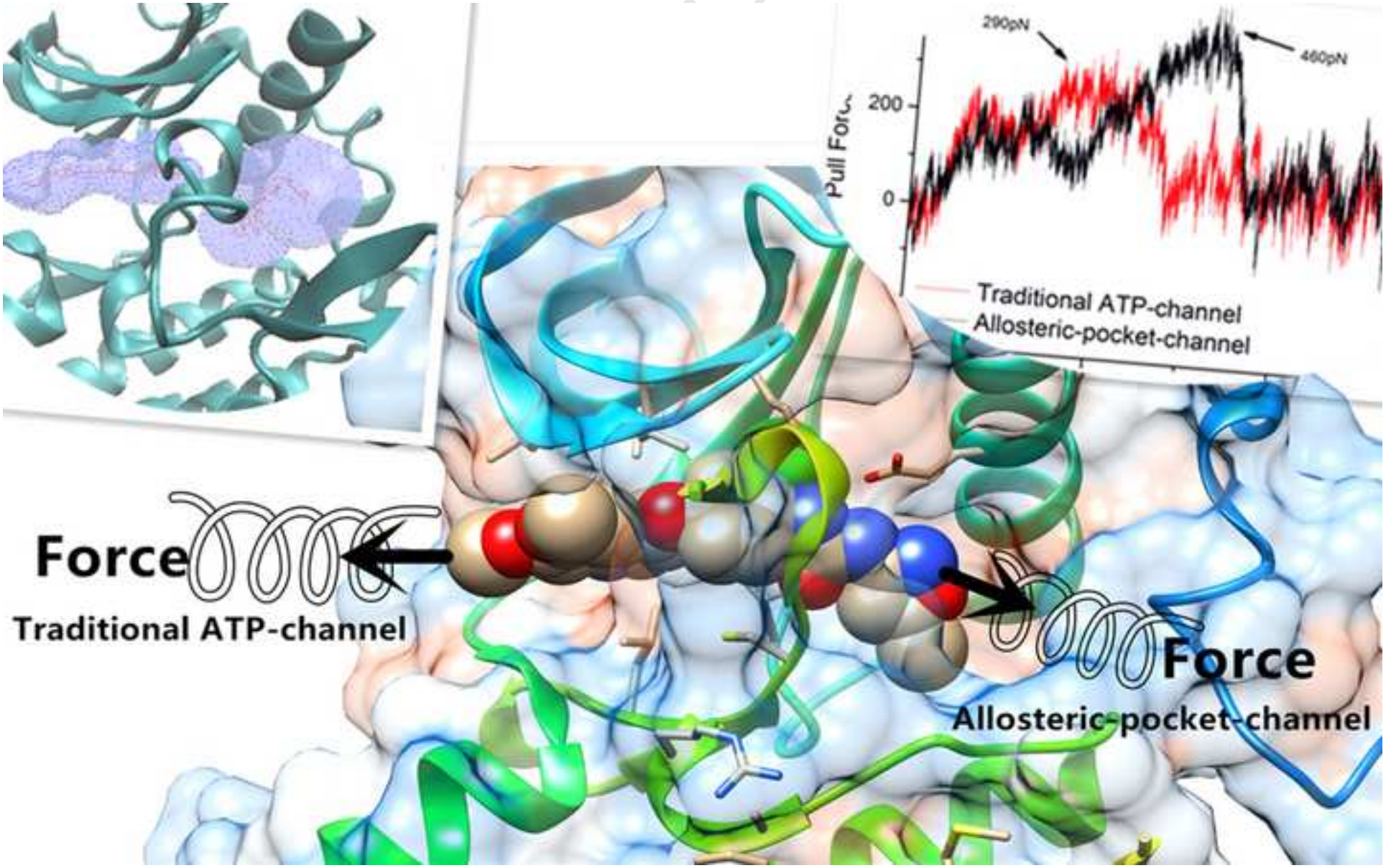

ACCEPTED MANUSCRIPT

Highlights,

1) We used the method of drug design based on the fragment-build method.
2) Traditional MD simulations were used to obtain the stable conformation.
3) SMD simulation were conducted to identify which path is the favorable unbinding path.
4) SMD simulation along with the two directions of the pocket were performed.

Accepted Manuscript

*Revised Manuscript

The Unbinding Mechanism Studies of Vascular Endothelial Growth Factor Receptors-2 Protein Tyrosine Kinase Type Ⅱ Inhibitors

Cong-min KANG [1] Dong-qing LIU [1] Xin-ying WANG [1] Ri-lei YU [2]

Ying-tao LV [1, *]

([1] College of Chemical Engineering, Qingdao University of Science and Technology, Qingdao 266042, P. R. China

[2] School of Pharmacy, Ocean University of China, Qingdao 266003, P. R. China)

Abstract: Vascular endothelial growth factor receptor-2 (VEGFR-2) tyrosine kinase has two conformations, active and inactive conformations. Type II inhibitors bind to inactive conformation. It has two possible binding/unbinding paths. To explore the unbinding path of inhibitor 01-435 that was generated by fragment build in the binding pocket of VEGFR-2, molecular dynamics (MD) simulation was performed on the crystal structure of VEGFR-2 in complex with 01-435, then steered molecular dynamics (SMD) simulation was executed on the crystal structure of VEGFR-2 in complex with 01-435. Pull force, van der Waals and electrostatic interaction along the two paths were calculated by using SMD simulation. The SMD simulation results indicate that the more favorable path for inhibitor dissociation is along with the traditional ATP-channel rather than the allosteric-pocket-channel, which is mainly due to the less electrostatic interaction that the ligand suffers during dissociation process along the traditional ATP-channel.

Key Words: VEGFR-2; SMD; Fragment build; Pull force; Electrostatic interaction

1 Introduction

Vascular endothelial growth factor (VEGF) is one of the key players in angiogenesis[1-3], and is thought to exert its angiogenic effect via binding to its receptor (VEGF receptor-2 protein tyrosine kinase, VEGFR-2 PTK) on the surface of endothelial cells[4]. VEGFR-2 has been proved to be the principal mediator in tumor angiogenesis[5-7], which is crucial for solid tumor development[8]. Therefore, VEGFR-2 PTK is recognized as the target for the development of therapeutic drugs against angiogenesis[9].

VEGFR-2 belongs to protein tyrosine kinase family, which consists of an N-terminal lobe and an C-terminal lobe[10], and a short strand termed the hinge region connecting the two lobes[11]. The ATP binding site is sandwiched between the lobes where ATP forms critical hydrogen bonding interactions to the hinge region[12]. The N-terminal of the activation loop contains an invariant Asp-Phe-Gly (DFG)

* Corresponding author. Tel: +86 53284023290, Email: lvyingtao@qust.edu.cn

motif[13], and in the DFG motif , the direction of benzene ring on the Phenylalanine determines the activity (“DFG-in”) or inactive (“DFG-out”) conformations of the enzyme. Kinase inhibitors that bind to the active form of the kinase are often called type I inhibitors, and those that bind to the inactive form of the kinase are called type II inhibitors[14]. Compared to type I inhibitors , type II inhibitors have a variety of advantages, which include better biochemical efficiency and higher selectivity[15].

Fig.1 shows type II inhibitors occupy both the traditional ATP-binding pocket and the allosteric pocket[16]. It appears that there are two possible paths for the binding/unbinding of type II inhibitors: one is along with the traditional ATP-channel and the other is the allosteric-pocket-channel[17]. Here, we will compare both paths and the better one will be confirmed. The gray area shows the pocket radius that we used MolCal software[18] to calculate in Fig.1. This picture shows that the allosteric-pocket-channel might be favored since this channel is relatively wider than the traditional ATP-channel. In this article, steered molecular dynamics[19, 20] were conducted to clarify this mechanism. Based on the small molecule inhibitor 01-435(Fig.2) that the laboratory found by fragment build[21], cv-SMD simulation[22] was used to pull the small molecular inhibitor 01-435 out of the allosteric site to explore the possible dissociation channel of type II kinase inhibitors.

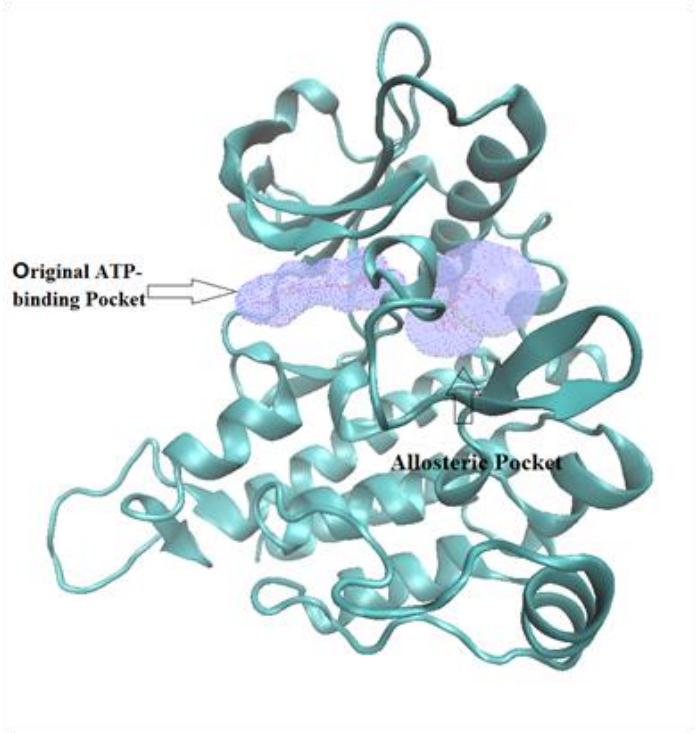

Fig.1 The chemical structure of VEGFR-2

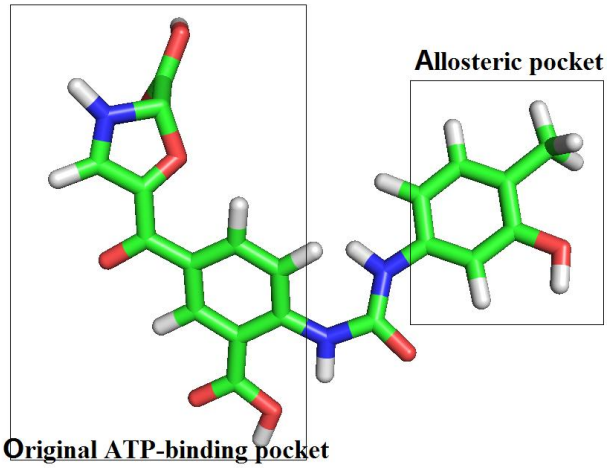

Fig.2 The structure of type II inhibitor 01-435

2 Methodology

Crystal structure of VEGFR-2 PTK in complex with ligand AV9 (PDB ID: 4ASE[23]) were obtained from the Protein Data Bank (PDB)[24]. Missing atoms in protein were added using Chimera[25] and Modeller[26].

Fragment build of inhibitor 01-435

Fragment build based on the structure of receptor 4ASE was used to generate new compounds, and LigBuilder V2.0[27] was applied to conduct fragment build. To examine ADME/Tox[28] of the new molecules, FAF-Drugs2[29], a free adaptable tool for ADME/Tox filtering of electronic compound collections was used. The filtering rules for acceptable physicochemical properties were set as follow: the well-known Lipinski's rule-of-five[30]: MW: 100 - 600, logP: -3 to 6, HBA≤12, HBD ≤ 5, and tPSA ≤ 180, Rotatable Bonds ≤ 11, Rigid Bonds ≤ 30, Rings ≤ 6, MaxSize System Ring ≤ 18, Carbons: 3-35, Hetero Atoms: 1-15, H/C Ratio: 0.1-1.1, Charges ≤ 3, Total Charge: -2 to 2. The molecules that passed ADME/Tox and two drugs (Sorafenib、Axitinib)[31] were selected as ligands. Then VEGFR-2 tyrosine kinase was selected as receptor. Each ligand was docked into the receptor using Autodock Vina[32], and the binding energy was obtained, respectively[33]. The compound containing the lowest binding energy was selected to conduct the MD and SMD simulation.

Traditional MD simulation

All structures were initially prepared with the Visual Molecular Dynamics package (VMD) [34] and all simulations were performed with GROMACS[35, 36] using the GROMOS96 43A force field. The inactive conformation with inhibitor complexes were immersed in the cuboid box filled with water molecules at a distance of 1 nm away from the box wall. The electroneutrality of the system was achieved by adding one Na^+ ion. A flexible SPC water model was used in the energy minimization step. The linear constraint solver algorithm was applied to constrain the bond lengths with a simulation time step of 2 fs to integrate the equation of motion for all atoms.

Electrostatic interactions were considered to use the Particle-Mesh Ewald (PME) algorithm[37, 38]with a distance cut off of 1.2 nm. Following minimization, 1000 ps of constant volume-temperature (NVT) MD simulation and constant pressure -temperature (NPT) MD simulation were performed to equilibrate the system. Finally, a total 30 ns MD simulation was implemented on the whole system to ensure the accomplishment of the equilibrium[39].

Steered MD and Umbrella Sampling

Furthermore, SMD simulation[40] was conducted by choosing the stabilized structure obtained from traditional molecular dynamics simulation[41]. SMD simulation along with the two directions of the pocket were performed, one along with the traditional ATP-channel, the other along with the allosteric-pocket-channel. Prior to MD simulation we estimated the pKa values of the residues in the protein using PROPKA webserver (http://nova.colombo58.unimi.it/propka.htm). And the protonate states of the residues were assigned based on their pKa at physiological pH. The spring constant was set to the value of 1000 kcal/mol·nm^2 with a pulling velocity of 0.001 nm/ps. Subsequently, a constant velocity was applied to the mass center of the 01-435 pulling the ligand 3 nm away, effectively into bulk solvent. Finally, two results of SMD simulation were analyzed.

3 Results and Discussion

Generation and screening of new molecules

1001 new molecules were obtained by running LigBuilder V2.0. Out of these molecules, 58 molecules remained after ADME/Tox screening. Finally molecular docking was conducted to get the binding energies of these 60 molecules (Table 1). The compound 01-435 with VEGFR-2 tyrosine kinase has the lowest binding energy which was lower than the binding energy of sorafenib, so it was selected to conduct the MD and SMD simulations.

Table 1 Docking Energy

Ligand	Binding Affinity	Ligand	Binding Affinity
4ase_01_435	-11.9	4ase_31_001	-8.2
4ase_ sorafenib	-10.2	4ase_06_082	-8.1
4ase_01_438	-10	4ase_01_379	-8
4ase_06_020	-9.3	4ase_33_001	-8
4ase_01_422	-9.2	4ase_33_004	-7.8
4ase_09_036	-9.2	4ase_01_410	-7.6
4ase_01_296	-9.1	4ase_01_470	-7.5
4ase_01_483	-9	4ase_11_002	-7.5
4ase_01_349	-8.9	4ase_axitinib	-7.5
4ase_01_257	-8.8	4ase_27_001	-7.4
4ase_01_385	-8.8	4ase_27_002	-7.4
4ase_01_436	-8.8	4ase_27_003	-7.4
4ase_01_095	-8.7	4ase_27_004	-7.4
4ase_26_001	-8.7	4ase_01_019	-7.3

4ase_31_003	-8.7	4ase_01_297	-7.3
4ase_32_001	-8.7	4ase_01_387	-7.3
4ase_32_002	-8.7	4ase_01_432	-7.3
4ase_01_047	-8.6	4ase_19_007	-7.2
4ase_33_002	-8.6	4ase_01_021	-7.1
4ase_01_180	-8.5	4ase_01_073	-7.1
4ase_01_392	-8.5	4ase_01_203	-7.1
4ase_06_098	-8.4	4ase_01_309	-7.1
4ase_31_002	-8.4	4ase_01_481	-7.1
4ase_01_092	-8.3	4ase_01_351	-7
4ase_01_087	-8.2	4ase_01_471	-7
4ase_01_192	-8.2	4ase_03_011	-7
4ase_01_476	-8.2	4ase_06_085	-7
4ase_06_066	-8.2	4ase_12_011	-7
4ase_25_002	-8.2	4ase_01_428	-6.9

Which is the favored channel of ligand 01-435 dissociation

After 30 ns traditional MD simulation for the crystal structure of VEGFR-2 in complex with 01-435, the RMSD changement of VEGFR-2 tyrosine kinase backbone atoms was shown in Fig.3. In this figure, the system of the complex reached equilibration after 18ns. Then the SMD simulation was carried out, in which initial structure was the snapshots randomly taken from the equilibration states in the traditional molecular dynamics.

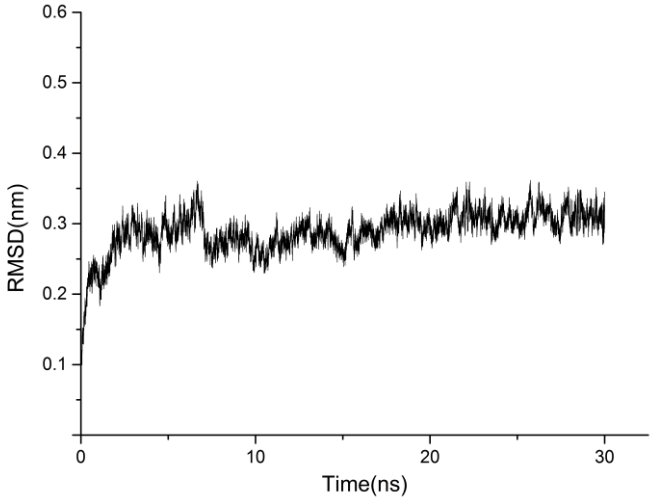

Fig.3 RMSD change of VEGFR-2 tyrosine kinase backbone atoms in MD simulation

Fig.4 shows the pull forces as a function of the end-to-end distance obtained with stretching velocity 0.001nm/ps. The red line describes the pull force along the traditional ATP-channel, the black line represents the pull force in allosteric-pocket-channel. Clearly, increased force appeared when the ligand 01-435

began to move out of the binding site, which indicated that the ligand encountered energy barriers when it passed through DFG motif. The maximum pulling forces are 290pN and 460pN for the traditional ATP-channel and allosteric-pocket-channel, respectively. Apparently, the inhibitor suffers a smaller force when dissociated along the traditional ATP-channel than along the allosteric-pocket-channel.

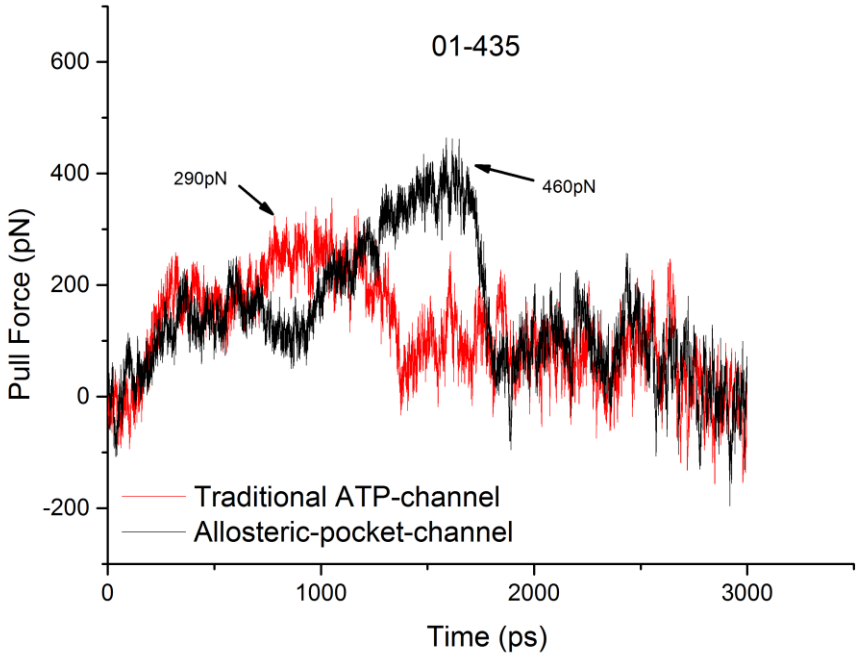

Fig.4 The pull force profiles of inhibitor unbinding along traditional ATP-channel (red) and allosteric-pocket-channel (black).

The analysis of dissociation path

Why the dissociation of the ligand through the traditional ATP-channel is more favored? In order to address this question, the key components of interaction between the ligand and protein kinases during SMD simulation were analyzed, including pull force, hydrogen bonds, van der Waals' force (VDW) and electrostatic interaction. Here g_mmpbsa[42] was carried out to calculate the VDW and electrostatic interactions. As shown in Fig.4, there is a peak in each dissociation path, which means that the ligand needs the maximum pull force to dissociate. Then complex conformation was gotten when the maximum force appeared under dissociation paths of two directions. Fig.5 (a) shows that with the ligand unbinding along the traditional ATP-channel, the complex conformation formed when the largest pull force appeared. Fig.5 (b) shows that with the ligand unbinding along the allosteric-pocket-channel, the complex conformation formed when the largest pull force appeared. In Fig.5 (a), six hydrogen bonds were shown, which were formed between the ligand and the amino residue, including Asn117, Lys62 and Asp190. However, in Fig.5 (b), seven hydrogen bonds were formed along the allosteric-pocket-channel dissociation, respectively with

Lys62, Glu79, Asp190 and Leu193. Take the position of ligand relative to DFG-motif into consideration, with the ring structure, the largest pull force appeared through the DFG-motif. But the simple comparison of these, it is difficult to determine the cause why the ligand tends to dissociate along the traditional ATP-channel.

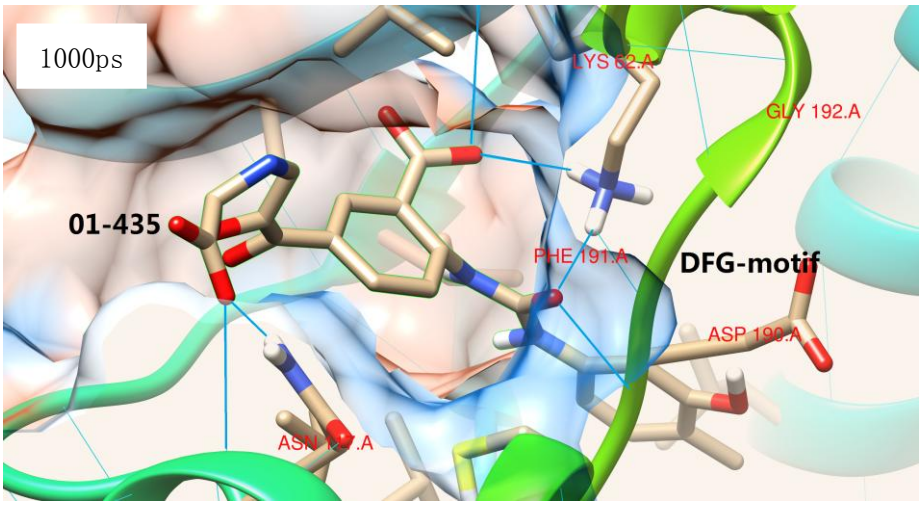

a) Traditional ATP-channel (1000ps)

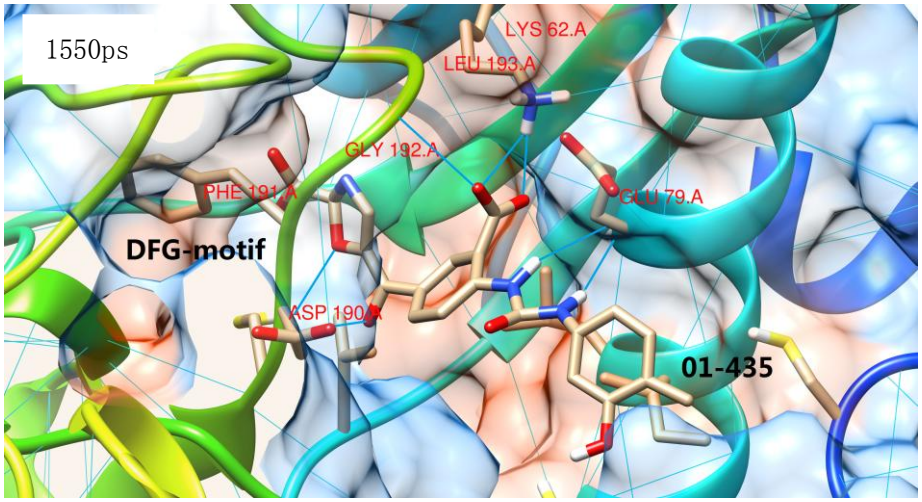

b) Allosteric-pocket-channel (1550ps)

Fig.5 Snapshots of the complex at the largest pull force

Fig.6, 7 and 8 display the vdW interactions, hydrogen bonds and electrostatic interactions between the protein and ligand during the dissociation, respectively. Figures shown in red line are for the traditional ATP-channel and those shown in black line are for the allosteric-pocket-channel. The energy of vdW interaction (Fig.6) is about -220kJ/mol while the energy of electrostatic interactions (Fig.8) is about -580 kJ/mol. Obviously, the energy of vdW interaction is higher compared with electrostatic interactions. And the fluctuations have some similarities for both paths, they have almost no significance to compare. The energy fluctuations of vdW interaction and the pull force have little correlation.

The number of hydrogen bonds and electrostatic interactions were analyzed, expecting to find out the reasons for the pull force differences.

Fig.7 presents the hydrogen bonds between the inhibitors and protein through two different dissociation paths. When the inhibitor dissociates through the allosteric-pocket-channel, the time point for the highest hydrogen bonds number peak is around 1550ps. And when inhibitor dissociates through traditional ATP-channel, the time point for the highest hydrogen bonds number peak is around 1000ps. Compared with the pull force profiles (Fig.4), this is consistent with the time when the ligand suffered the maximum pull force. In other words, the fluctuation of pull force is related to the number of hydrogen bonds.

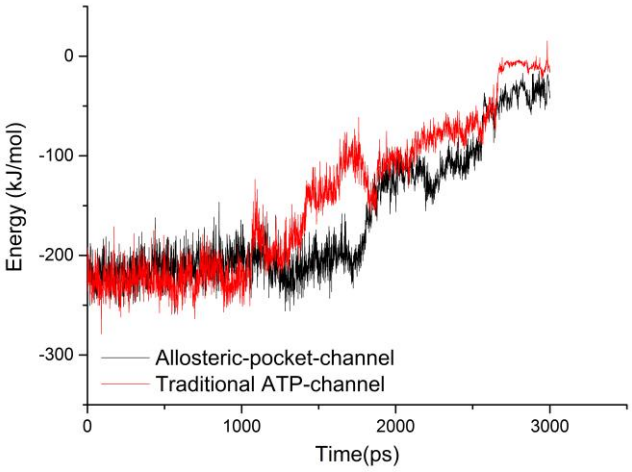

Fig.6 Energy profiles of vdW interaction during the dissociation

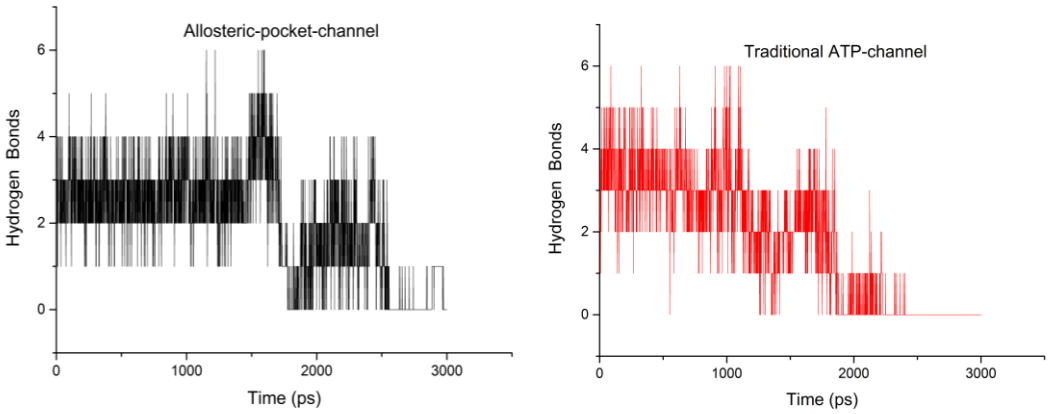

Fig.7 Number of hydrogen bonds over the simulation time

At last, the electrostatic interactions for the both paths were analyzed. We were surprised to find that the fluctuation of electrostatic interactions and the pull force were very similar. In 1000ps, for traditional ATP-channel, the electrostatic interactions reached the maximum, where the pull force was highest, however for allosteric-pocket-channel the electrostatic interactions were relatively weak and the pull force was relatively low. It indicates that the energy of electrostatic interactions

has a great influence on pull force. The energy of electrostatic interactions for allosteric-pocket-channel reached the maximum 1150kJ/mol in 1550ps, much higher than the energy of traditional ATP-channel which is 940kJ/mol in 1000ps. Hence, the energy barrier of pull force for allosteric-pocket-channel is higher than traditional ATP-channel. This is the main reason why the ligand dissociation through the traditional ATP-channel is more favored.

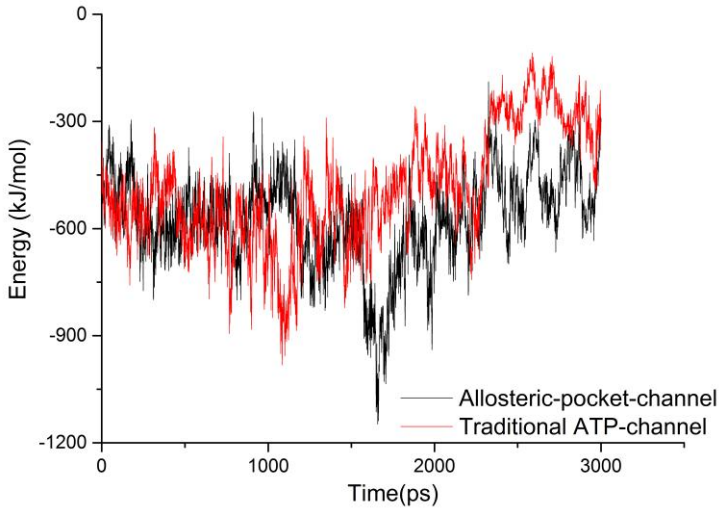

Fig.8 Energy profiles of electrostatic interaction during the dissociation

4 Conclusions

In this study, *de novo* design based on receptors was conducted to get VEGFR-2 tyrosine kinase type II inhibitor 01-435. For the complex of 01-435 with VEGFR-2 tyrosine kinase, traditional MD simulation and SMD simulation were executed to investigate the unbinding mechanisms of the two different dissociation paths. Pull force, hydrogen bonds, vdW and electrostatic interactions of the two dissociation paths have been calculated by SMD simulation. In pull force analysis, two paths reach a peak at the time point 1000ps and 1550ps, respectively. The maximum pull force is 290pN for the traditional ATP-channel while it is 460pN for allosteric-pocket-channel. Apparently, the inhibitor suffered a smaller force when dissociation along the traditional ATP-channel than along the allosteric-pocket-channel. This means the traditional ATP-channel is favored for ligand dissociation. By analyzing the number of hydrogen bonds, vdW and electrostatic interactions, we find the main reasons that influence pull force are hydrogen bonds and electrostatic interactions. The information obtained here can be used to direct the discovery of type II kinase inhibitors. Applications of the SMD method to investigate the unbinding mechanism would be an interesting subject in the future.

Acknowledgement

The project was supported by the National Natural Science Foundation of China

(21272131) and Shandong Provincial Natural Science Foundation, China (ZR2011BM015).

Reference

[1] M.A. Shah, Z.A. Wainberg, D.V. Catenacci, H.S. Hochster, J. Ford, P. Kunz, F.-C. Lee, H. Kallender, F. Cecchi and D.C. Rabe. Phase II study evaluating 2 dosing schedules of oral foretinib (GSK1363089), cMET/VEGFR2 inhibitor, in patients with metastatic gastric cancer. PloS one. 8 (2013) e54014.

[2] D. Li, K. Xie, G. Ding, J. Li, K. Chen, H. Li, J. Qian, C. Jiang and J. Fang. Tumor resistance to anti-VEGF therapy through up-regulation of VEGF-C expression. Cancer Lett. 346 (2014) 45-52.

[3] M. Shibuya. Vascular endothelial growth factor and its receptor system: physiological functions in angiogenesis and pathological roles in various diseases. J. Biochem. 153 (2013) 13-19.

[4] D.J. Hicklin and L.M. Ellis. Role of the vascular endothelial growth factor pathway in tumor growth and angiogenesis. J. Clin. Oncol. 23 (2005) 1011-1027.

[5] M. Scartozzi, R. Giampieri, C. Loretelli, A. Bittoni, A. Mandolesi, L. Faloppi, M. Bianconi, M. Del Prete, K. Andrikou, I. Bearzi and S. Cascinu. Tumor angiogenesis genotyping and efficacy of first-line chemotherapy in metastatic gastric cancer patients. Pharmacogenomics. 14 (2013) 1991-1998.

[6] S.W. Huang, J.C. Lien, S.C. Kuo and T.F. Huang. PPemd26, an anthraquinone derivative, suppresses angiogenesis via inhibiting VEGFR2 signalling. Br. J. Pharmacol. 171 (2014) 5728-5742.

[7] N. Ferrara and R.S. Kerbel. Angiogenesis as a therapeutic target. Nature. 438 (2005) 967-974.

[8] D.A. Cheresh and D.G. Stupack. Tumor Angiogenesis Putting a Value on Plastic GEMMs. Circ. Res. 114 (2014) 9-11.

[9] J. Gille. Antiangiogenic cancer therapies get their act together: current developments and future prospects of growth factor‐and growth factor receptor‐targeted approaches. Experimental dermatology. 15 (2006) 175-186.

[10] M.B. Lamers, A.A. Antson, R.E. Hubbard, R.K. Scott and D.H. Williams. Structure of the protein tyrosine kinase domain of C-terminal Src kinase (CSK) in complex with staurosporine. J. Mol. Biol. 285 (1999) 713-725.

[11] J.A. Bikker, N. Brooijmans, A. Wissner and T.S. Mansour. Kinase domain mutations in cancer: implications for small molecule drug design strategies. J. Med. Chem. 52 (2009) 1493-1509.

[12] L.R. Masterson, C. Cheng, T. Yu, M. Tonelli, A. Kornev, S.S. Taylor and G. Veglia. Dynamics connect substrate recognition to catalysis in protein kinase A. Nat. Chem. Biol. 6 (2010) 821-828.

[13] S. Han, A. Mistry, J.S. Chang, D. Cunningham, M. Griffor, P.C. Bonnette, H. Wang, B.A. Chrunyk, G.E. Aspnes and D.P. Walker. Structural characterization of proline-rich tyrosine kinase 2 (PYK2) reveals a unique (DFG-out) conformation and enables inhibitor design. J. Biol. Chem. 284 (2009) 13193-13201.

[14] Y. Liu and N.S. Gray. Rational design of inhibitors that bind to inactive kinase conformations. Nat. Chem. Biol. 2 (2006) 358-364.
[15] Q. Zhang, Y. Diao, F. Wang, Y. Fu, F. Tang, Q. You and H. Zhou. Design and discovery of 4-anilinoquinazoline ureas as multikinase inhibitors targeting BRAF, VEGFR-2 and EGFR. MedChemComm. 4 (2013) 979-986.
[16] P.M.-U. Ung and A. Schlessinger. DFGmodel: Predicting Protein Kinase Structures in Inactive States for Structure-Based Discovery of Type-II Inhibitors. ACS Chem. Biol. 10 (2015) 269-278.
[17] L.-J. Yang, J. Zou, H.-Z. Xie, L.-L. Li, Y.-Q. Wei and S.-Y. Yang. Steered molecular dynamics simulations reveal the likelier dissociation pathway of imatinib from its targeting kinases c-Kit and Abl. PloS one. 4 (2009) e8470.
[18] Q. Bai, H. Perez-Sanchez, Y. Zhang, Y. Shao, D. Shi, H. Liu and X. Yao. Ligand induced change of β2 adrenergic receptor from active to inactive conformation and its implication for the closed/open state of the water channel: insight from molecular dynamics simulation, free energy calculation and Markov state model analysis. Phys. Chem. Chem. Phys. 16 (2014) 15874-15885.
[19] B. Isralewitz, M. Gao and K. Schulten. Steered molecular dynamics and mechanical functions of proteins. Curr. Opin. Struct. Biol. 11 (2001) 224-230.
[20] B. Isralewitz, J. Baudry, J. Gullingsrud, D. Kosztin and K. Schulten. Steered molecular dynamics investigations of protein function. J. Mol. Graphics. Modell. 19 (2001) 13-25.
[21] E. Shang, Y. Yuan, X. Chen, Y. Liu, J. Pei and L. Lai. De Novo Design of Multitarget Ligands with an Iterative Fragment-Growing Strategy. J. Chem. Inf. Model. 54 (2014) 1235-1241.
[22] H.S. Martin, S. Jha and P.V. Coveney. Comparative analysis of nucleotide translocation through protein nanopores using steered molecular dynamics and an adaptive biasing force. J. Comput. Chem. 35 (2014) 692-702.
[23] M. McTigue, B.W. Murray, J.H. Chen, Y.-L. Deng, J. Solowiej and R.S. Kania. Molecular conformations, interactions, and properties associated with drug efficiency and clinical performance among VEGFR TK inhibitors. Proc. Natl. Acad. Sci. U S A. 109 (2012) 18281-18289.
[24] H.M. Berman, T. Battistuz, T. Bhat, W.F. Bluhm, P.E. Bourne, K. Burkhardt, Z. Feng, G.L. Gilliland, L. Iype and S. Jain. The protein data bank. Acta Crystallogr. D. Biol. Crystallogr. 58 (2002) 899-907.
[25] E.F. Pettersen, T.D. Goddard, C.C. Huang, G.S. Couch, D.M. Greenblatt, E.C. Meng and T.E. Ferrin. UCSF Chimera—a visualization system for exploratory research and analysis. J. Comput. Chem. 25 (2004) 1605-1612.
[26] N. Eswar, B. Webb, M.A. Marti‐Renom, M. Madhusudhan, D. Eramian, M.y. Shen, U. Pieper and A. Sali. Comparative protein structure modeling using Modeller2006.
[27] Y. Yuan, J. Pei and L. Lai. LigBuilder 2: a practical de novo drug design approach. J. Chem. Inf. Model. 51 (2011) 1083-1091.
[28] S. Ekins, B. Boulanger, P.W. Swaan and M.A.Z. Hupcey. Towards a new age of virtual ADME/TOX and multidimensional drug discovery. Mol. Divers. 5 (2002)

255-275.
[29] D. Lagorce, O. Sperandio, H. Galons, M.A. Miteva and B.O. Villoutreix. FAF-Drugs2: free ADME/tox filtering tool to assist drug discovery and chemical biology projects. BMC bioinformatics. 9 (2008) 396.
[30] T.H. Keller, A. Pichota and Z. Yin. A practical view of druggability. Curr. Opin. Chem. Biol. 10 (2006) 357-361.
[31] S.M. Keefe, M.A. Cohen and M.S. Brose. Targeting Vascular Endothelial Growth Factor Receptor in Thyroid Cancer: the Intracellular and Extracellular Implications. Clin. Cancer Res. 16 (2010) 778-783.
[32] G.M. Morris, R. Huey, W. Lindstrom, M.F. Sanner, R.K. Belew, D.S. Goodsell and A.J. Olson. AutoDock4 and AutoDockTools4: Automated docking with selective receptor flexibility. J. Comput. Chem. 30 (2009) 2785-2791.
[33] H. Jasuja, N. Chadha, M. Kaur and O. Silakari. Dual inhibitors of Janus kinase 2 and 3 (JAK2/3): designing by pharmacophore- and docking-based virtual screening approach. Mol. Divers. 18 (2014) 253-67.
[34] W. Humphrey, A. Dalke and K. Schulten. VMD: visual molecular dynamics. J. Mol. Graph. 14 (1996) 33-38.
[35] H.J. Berendsen, D. van der Spoel and R. van Drunen. GROMACS: A message-passing parallel molecular dynamics implementation. Computer Physics. Communications. 91 (1995) 43-56.
[36] D. Van Der Spoel, E. Lindahl, B. Hess, G. Groenhof, A.E. Mark and H.J. Berendsen. GROMACS: fast, flexible, and free. J. Comput. Chem. 26 (2005) 1701-1718.
[37] U. Essmann, L. Perera, M.L. Berkowitz, T. Darden, H. Lee and L.G. Pedersen. A smooth particle mesh Ewald method. J. Chem. Phys. 103 (1995) 8577-8593.
[38] T. Darden, D. York and L. Pedersen. Particle mesh Ewald: An N · log (N) method for Ewald sums in large systems. J. Chem. Phys. 98 (1993) 10089-10092.
[39] L. Minini, G. Alvarez, M. Gonzalez, H. Cerecetto and A. Merlino. Molecular docking and molecular dynamics simulation studies of Trypanosoma cruzi triosephosphate isomerase inhibitors. Insights into the inhibition mechanism and selectivity. J. Mol. Graphics. Modell. 58 (2015) 40-49.
[40] J. Jitonnom and C. Sontag. Comparative study on activation mechanism of carboxypeptidase A1, A2 and B: First insights from steered molecular dynamics simulations. J. Mol. Graphics. Modell. 38 (2012) 298-303.
[41] H. Lu and K. Schulten. Steered molecular dynamics simulations of force-induced protein domain unfolding. Proteins: Struct., Funct., Genet. 35 (1999) 453-463.
[42] R. Kumari, R. Kumar, O. Consortium and A.M. Lynn. g_mmpbsa-A GROMACS tool for high-throughput MM-PBSA calculations. J. Chem. Inf. Model. 54 (2014) 1951-1962.

ACCEPTED MANUSCRIPT

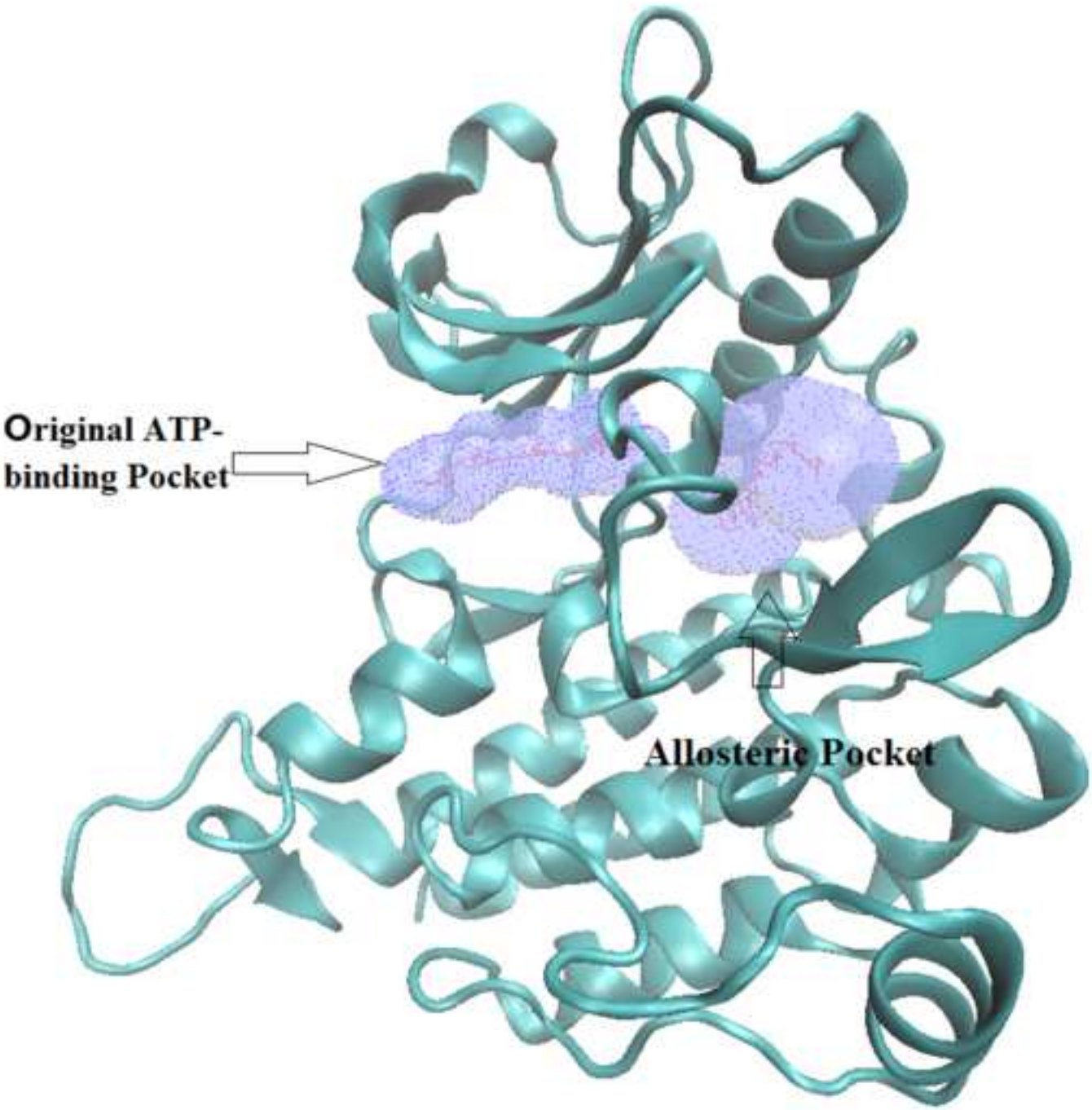

Figure(s)

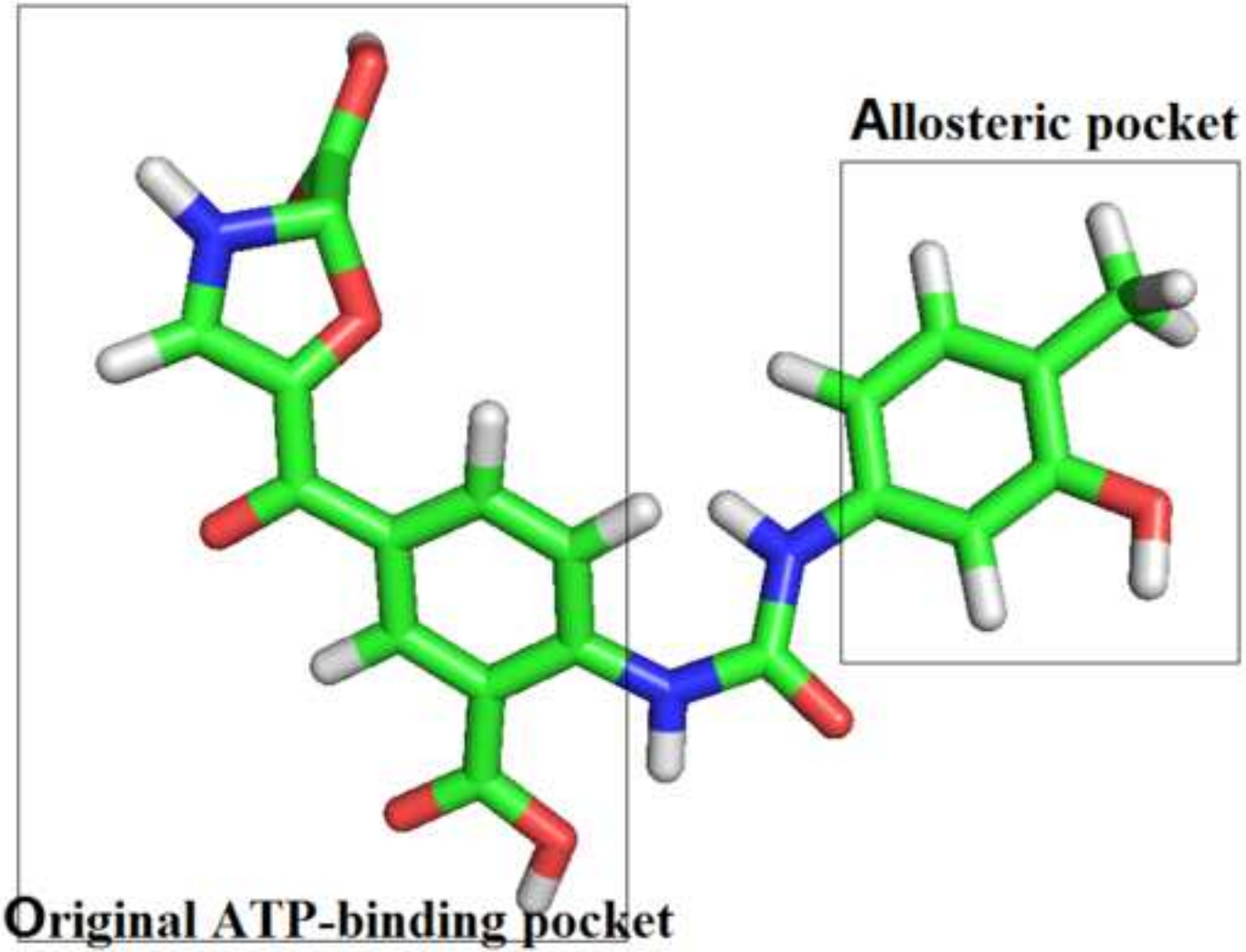

Figure(s)

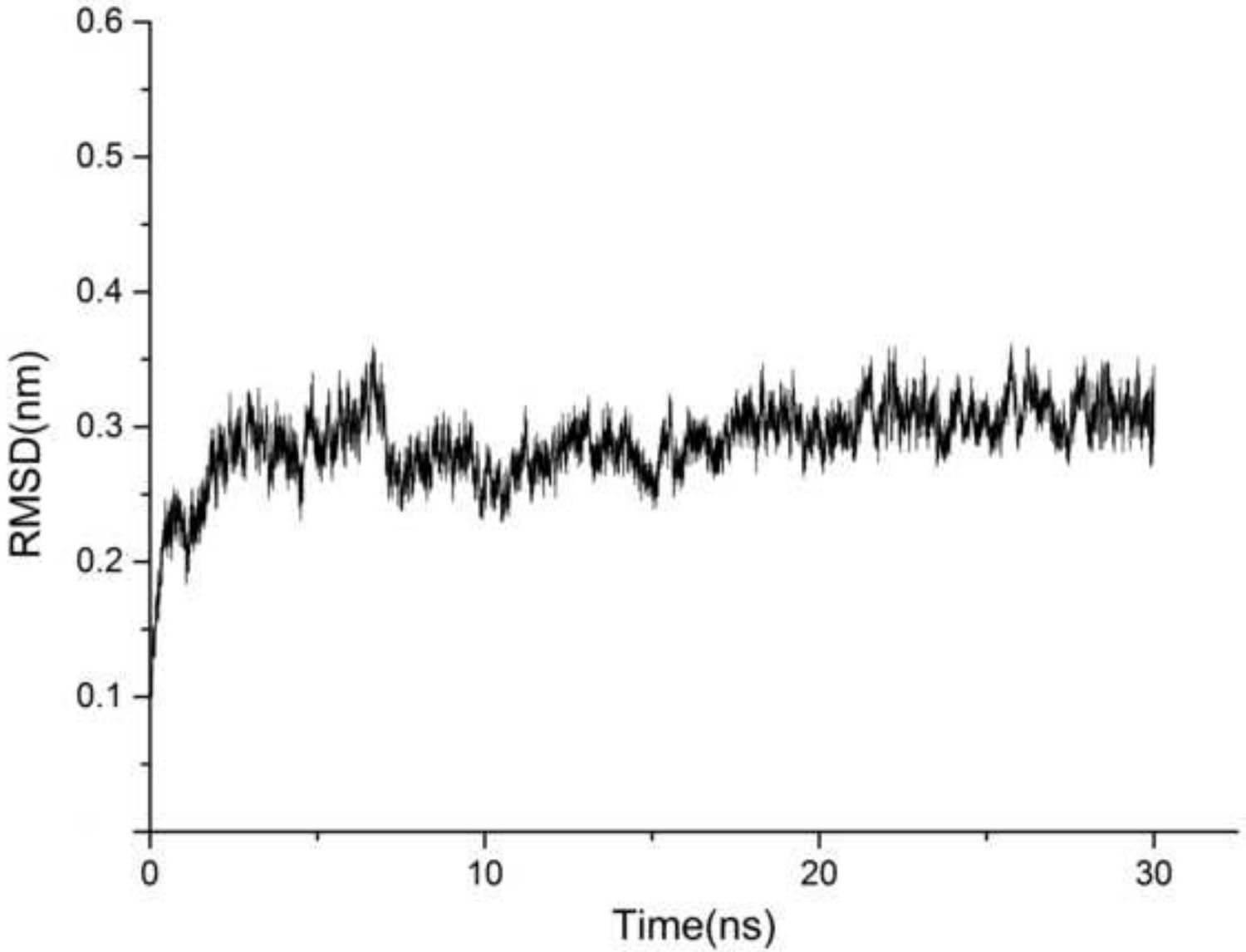

Figure(s)

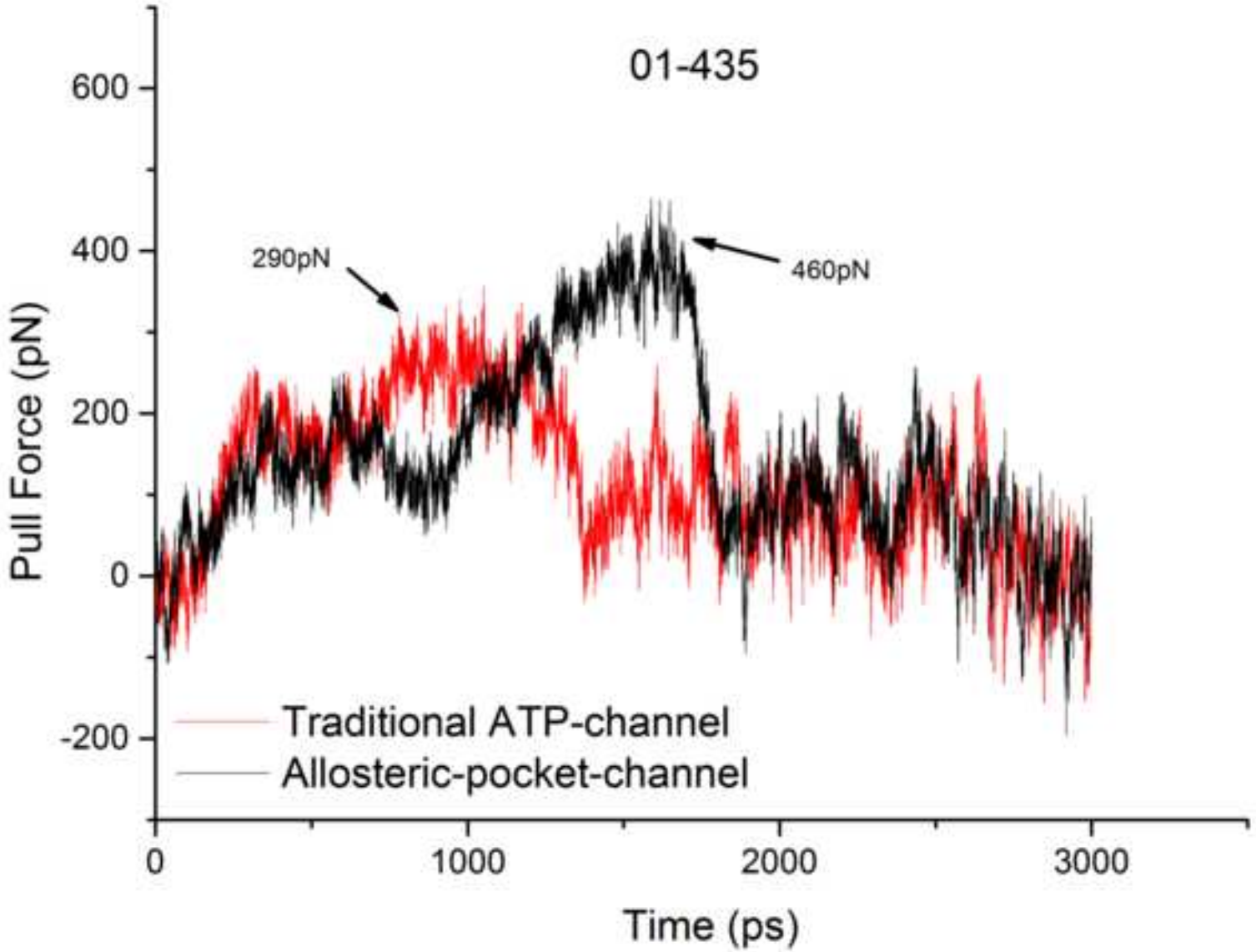
01-435
600
400
200
0
-200
Pull Force (pN)
290pN
460pN
Traditional ATP-channel
Allosteric-pocket-channel
0
1000
2000
3000
Time (ps)

Figure(s)

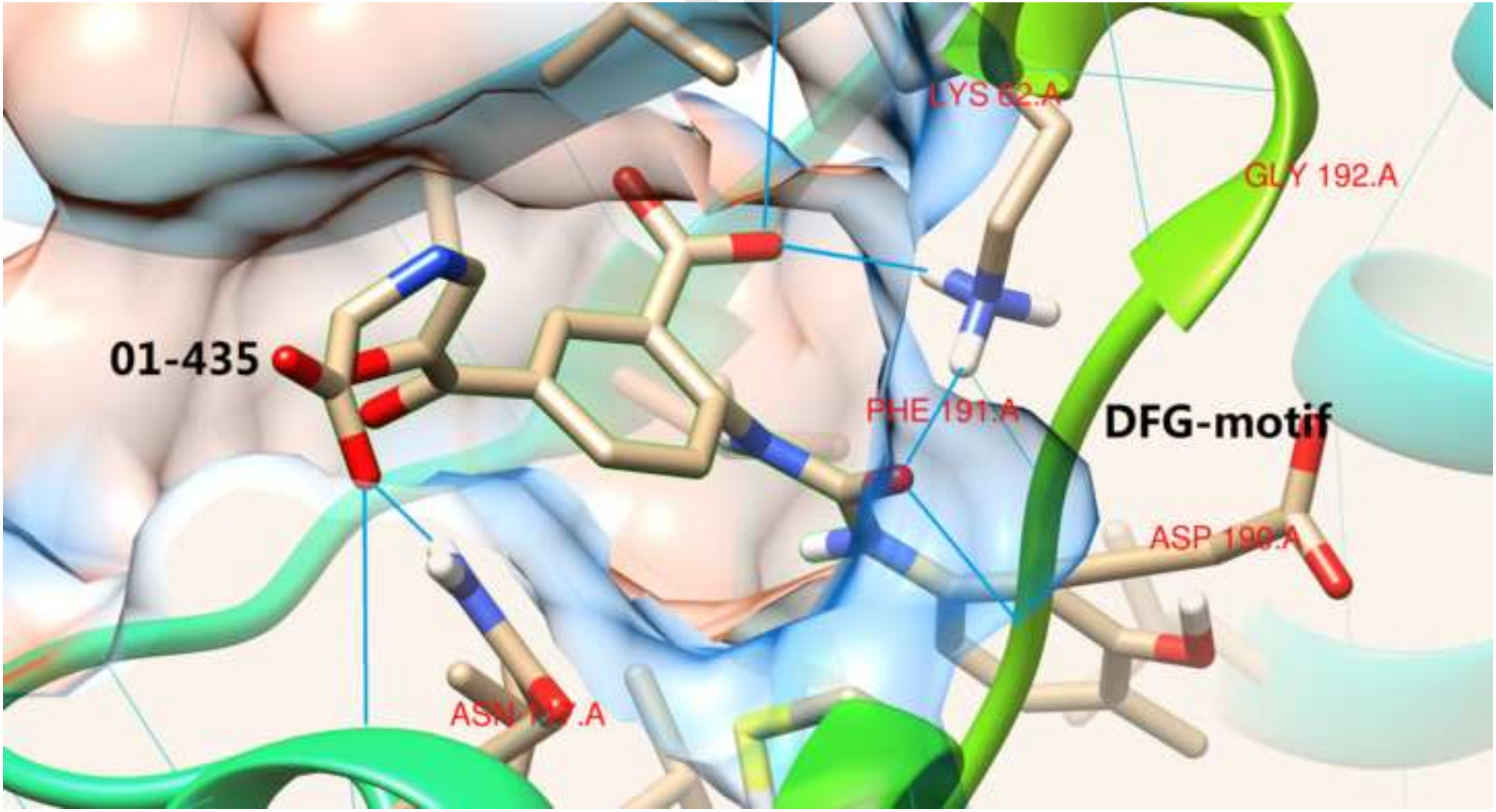

Figure(s)

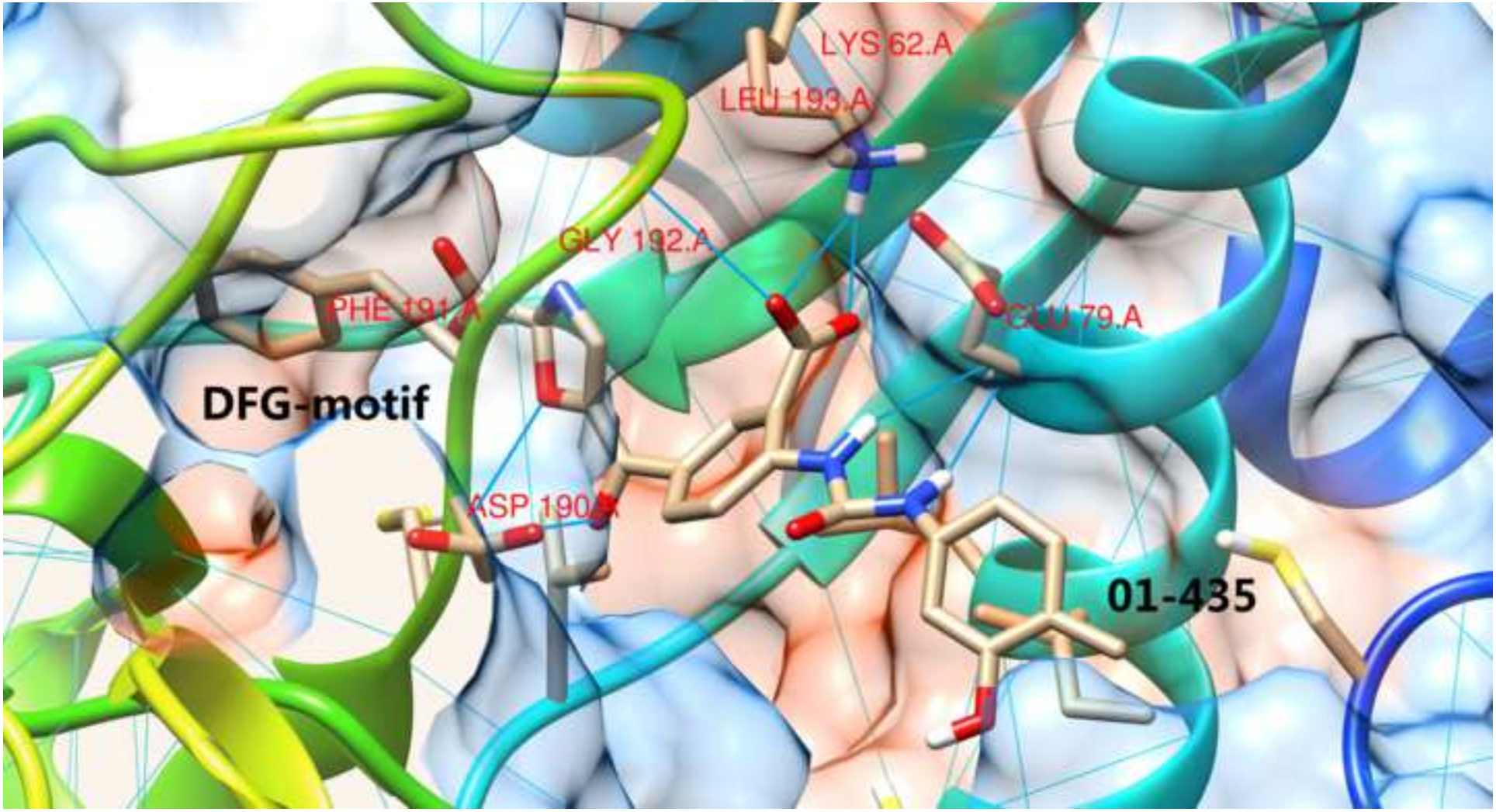
LYS 62.A
LEU 193.A
GLY 192.A
PHE 191.A
GLU 79.A
DFG-motif
ASP 190.A
01-435

Figure(s)

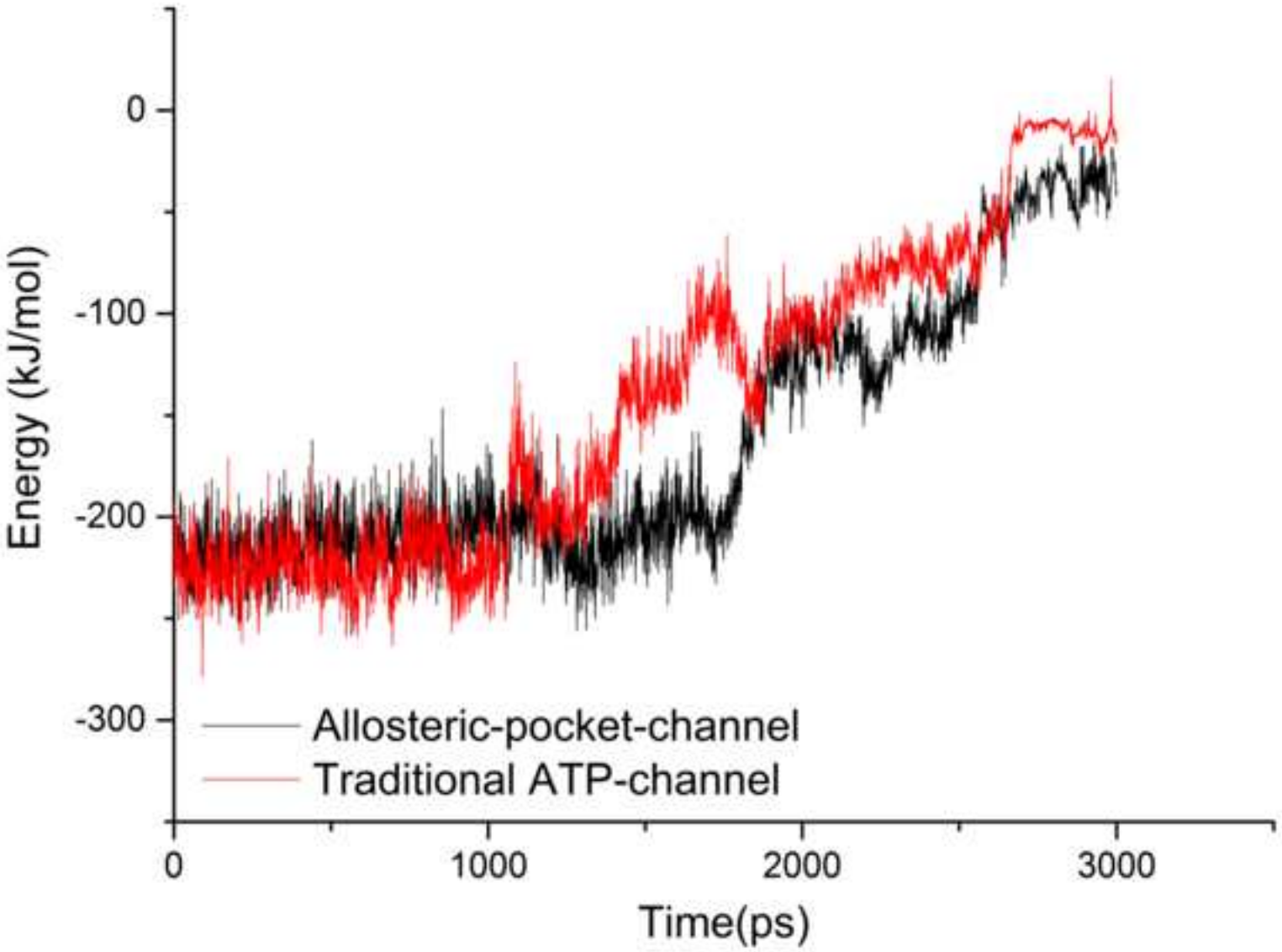
0
-100
-200
-300
Energy (kJ/mol)
0
1000
2000
3000
Time(ps)
Allosteric-pocket-channel
Traditional ATP-channel

Figure(s)

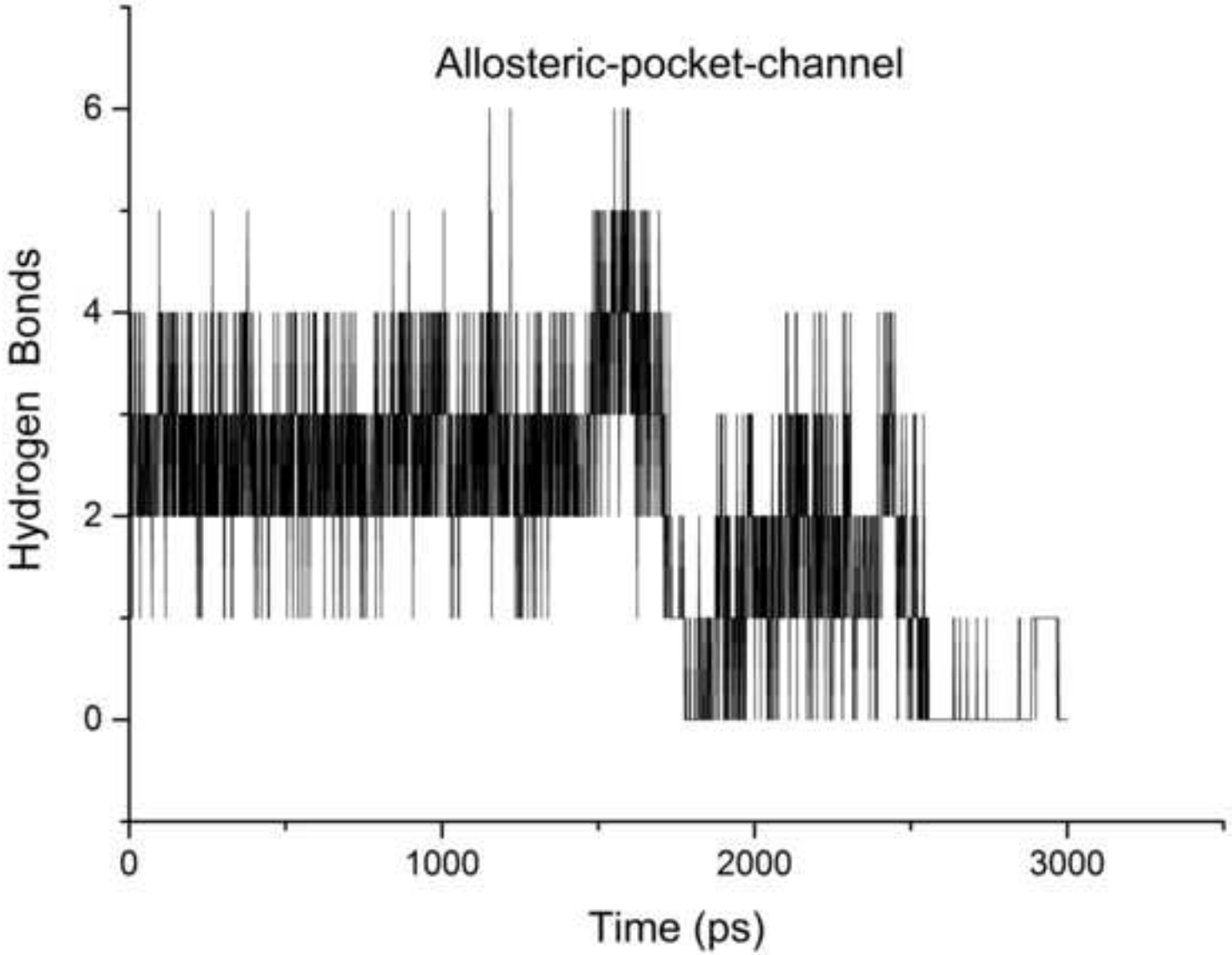
Allosteric-pocket-channel
Hydrogen Bonds
0
2
4
6
0
1000
2000
3000
Time (ps)

Figure(s)

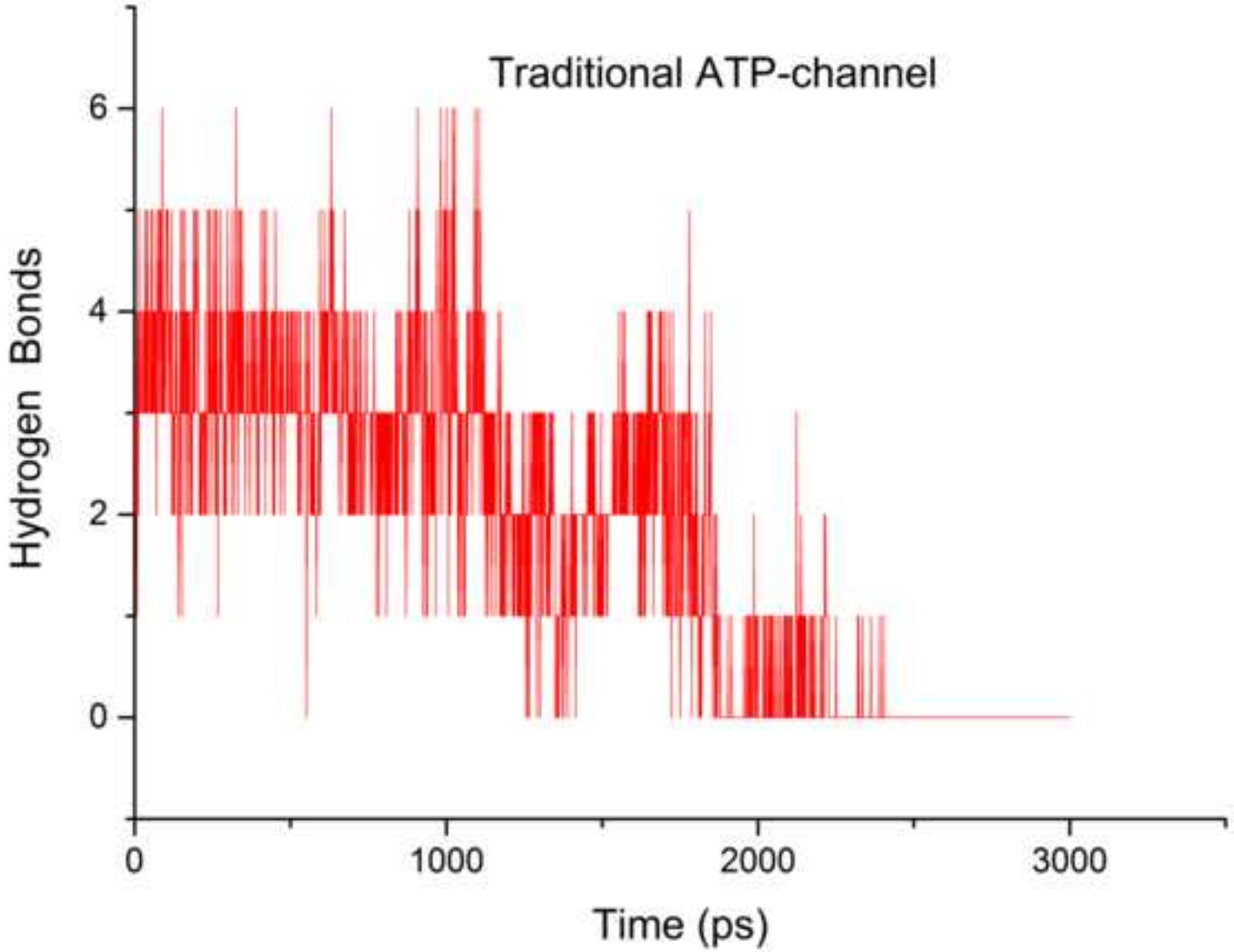
Traditional ATP-channel
Hydrogen Bonds
0
2
4
6
0
1000
2000
3000
Time (ps)

Figure(s)

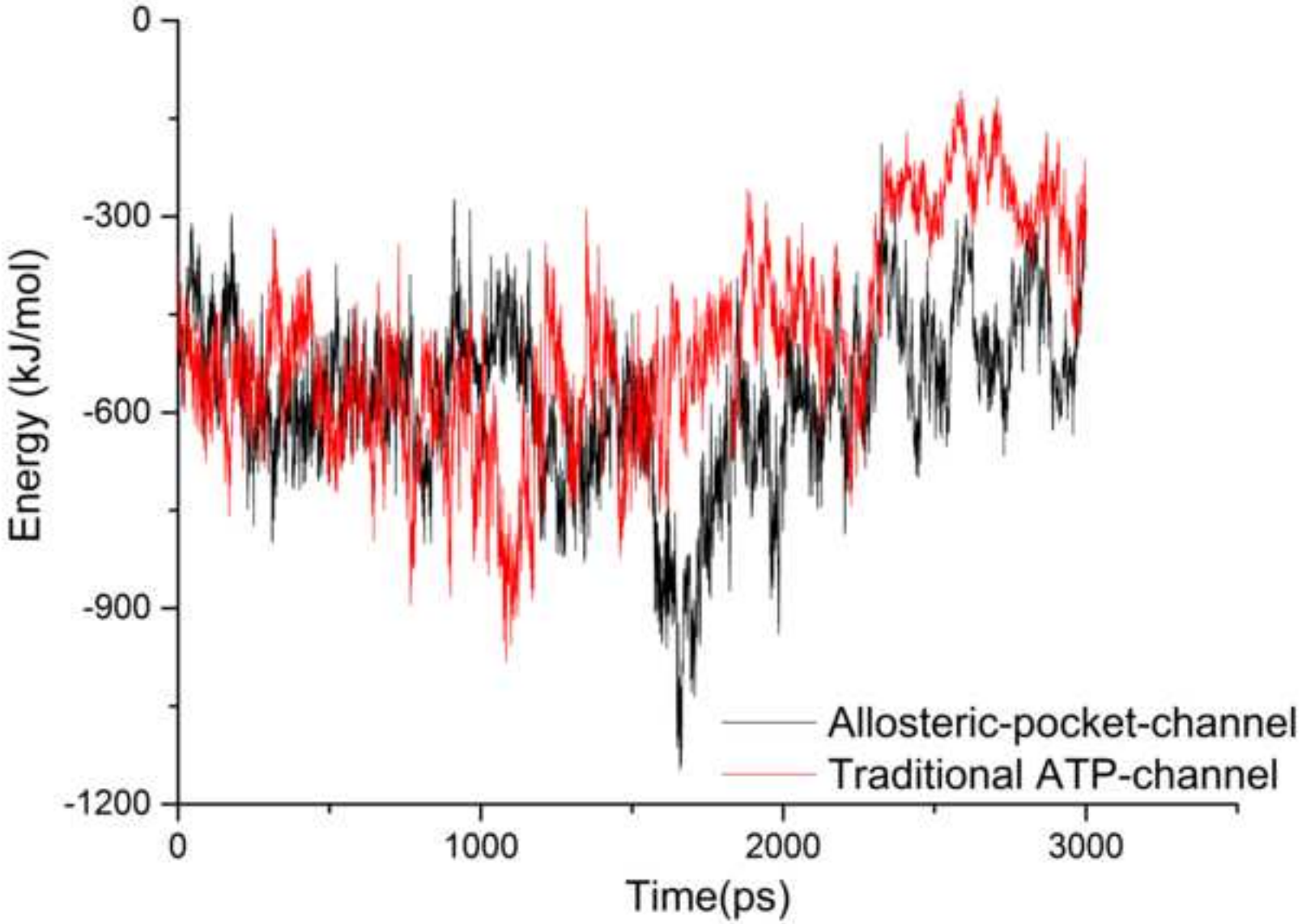
0
-300
-600
-900
-1200
Energy (kJ/mol)
0
1000
2000
3000
Time(ps)
Allosteric-pocket-channel
Traditional ATP-channel